© 2018. Published by The Company of Biologists Ltd | Journal of Experimental Biology (2018) 221, jeb177568. doi:10.1242/jeb.177568

RESEARCH ARTICLE

Cuticular gas exchange by Antarctic sea spiders

Steven J. Lane[1,*], Amy L. Moran[2], Caitlin M. Shishido[2], Bret W. Tobalske[1] and H. Arthur Woods[1]

ABSTRACT

Many marine organisms and life stages lack specialized respiratory structures, like gills, and rely instead on cutaneous respiration, which they facilitate by having thin integuments. This respiratory mode may limit body size, especially if the integument also functions in support or locomotion. Pycnogonids, or sea spiders, are marine arthropods that lack gills and rely on cutaneous respiration but still grow to large sizes. Their cuticle contains pores, which may play a role in gas exchange. Here, we examined alternative paths of gas exchange in sea spiders: (1) oxygen diffuses across pores in the cuticle, a common mechanism in terrestrial eggshells, (2) oxygen diffuses directly across the cuticle, a common mechanism in small aquatic insects, or (3) oxygen diffuses across both pores and cuticle. We examined these possibilities by modeling diffusive oxygen fluxes across all pores in the body of sea spiders and asking whether those fluxes differed from measured metabolic rates. We estimated fluxes across pores using Fick's law parameterized with measurements of pore morphology and oxygen gradients. Modeled oxygen fluxes through pores closely matched oxygen consumption across a range of body sizes, which means the pores facilitate oxygen diffusion. Furthermore, pore volume scaled hypermetrically with body size, which helps larger species facilitate greater diffusive oxygen fluxes across their cuticle. This likely presents a functional trade-off between gas exchange and structural support, in which the cuticle must be thick enough to prevent buckling due to external forces but porous enough to allow sufficient gas exchange.

KEY WORDS: Arthropod, Cuticle, Metabolism, Oxygen, Polar gigantism, Pycnogonids

INTRODUCTION

Many animals exchange some or all of their respiratory gases across their outer integument (i.e. skin or cuticle), a process known as cutaneous respiration (Graham, 1988; Feder and Burggren, 1985). The proportion of total gas exchanged across the outer integument varies across animals, especially among those that live in marine habitats (Feder and Burggren, 1985). Small animals, with relatively thin integuments and relatively low metabolic rates (e.g. flatworms and most marine larvae), rely on diffusion alone (Graham, 1988). By contrast, many larger marine organisms (e.g. many adult vertebrates and arthropods) have relatively thick integuments (skin or cuticle), such that oxygen diffusion alone cannot supply their higher metabolic rates, which are distributed throughout larger volumes. Instead, these groups often have specialized and highly ramified structures (e.g. gills), where most gas exchange occurs. Nevertheless, cutaneous respiration plays a role in all of these groups (Graham, 1988). For example, even in many adult fish, ∼30% of oxygen uptake occurs across the integument (Weibel et al., 1998). Therefore, understanding the mechanisms of cutaneous respiration is important to understanding the physiology of marine animals.

We studied cutaneous respiration in sea spiders (phylum Arthropoda, class Chelicerata). Sea spiders are a basal group in the Arthropoda (Arango and Wheeler, 2007) that lack specialized respiratory structures such as gills, but nevertheless can grow to substantial sizes (Moran and Woods, 2012; Child, 1995; Arnaud and Bamber, 1987; Dell, 1972). Sea spiders have reduced thoraces and abdomens and many of their metabolically active tissues, like guts and gonads, are distributed into their legs (Davenport et al., 1987), which reduces the distance oxygen must travel through the body by diffusion. Although sea spiders have been studied for over 150 years (see reviews by Arnaud and Bamber, 1987; King, 1973), we still lack an understanding of the functional morphology of the cuticle as it relates to gas exchange. An obvious possibility is that oxygen diffuses via the pores that appear to cross the cuticles of most species (Fahrenbach, 1994; Davenport et al., 1987; King, 1973), but this idea has never been tested. Here, we tested the role of cuticular pores in oxygen diffusion across the cuticle of sea spiders using a combination of empirical measurements and mathematical modeling.

There are several different avenues by which oxygen may cross the cuticle. First, as hypothesized by Davenport et al. (1987), oxygen may diffuse in through pores that cross the cuticle. In insects, the diffusion coefficient of oxygen through chitin is ∼4% that of the diffusion coefficient through water (Krogh, 1919), which is too low for adequate diffusive supply of oxygen unless the cuticle is extremely thin (e.g. ∼0.2–1.2 µm in the order Plecoptera; Resh et al., 2008). If the diffusion coefficient of oxygen through sea spider cuticle is similar to that of insect cuticle, then pores may permit much higher oxygen fluxes by reducing the amount of solid cuticle through which oxygen must diffuse. Pores in other cutaneous-respiring organisms appear to support almost all of the flux, especially when the integument is also used for support. For example, the pores in sea spiders are morphologically similar to those described from vertebrate and invertebrate eggshells (Rokitka and Rahn, 1987; Kern and Ferguson, 1997; Woods et al., 2005). These pores have been studied relatively extensively, and they do support almost all of the oxygen flux to the embryo (Wangensteen et al., 1971; Paganelli, 1980; Hinton, 1981; Tøien et al., 1988; Rahn and Paganelli, 1990).

Alternatively, cuticular pores may not facilitate oxygen flux; they may be incidental or have some other function (e.g. secretion). Cuticular pores have long been considered to have a secretory function (Fahrenbach, 1994), and it is possible they serve a dual function (secretion and gas exchange). Sea spiders are chelicerates, and the structure of chelicerate cuticle is, in general,

[1]Division of Biological Sciences, University of Montana, Missoula, MT 59812, USA. [2]Department of Biology, University of Hawai'i at Mānoa, Honolulu, HI 96822, USA.

*Author for correspondence (steven.lane@umontana.edu)

S.J.L., 0000-0002-3361-2244; B.W.T., 0000-0002-5739-6099; H.A.W., 0000-0002-3147-516X

Received 16 January 2018; Accepted 16 March 2018

Journal of Experimental Biology (2018) 221, jeb177568. doi:10.1242/jeb.177568

List of symbols and abbreviations

A_c	cross-sectional area of cuticle segment at top of pore (cm^2)
A_n	cross-sectional area of segment within pore (cm^2)
d	diameter of pore segment within model (cm)
d_c	diameter of top of pore
d_{20}	diameter of bottom of pore
D	diffusion coefficient
D_c	diffusion coefficient of oxygen in cuticle ($cm^2\ s^{-1}$)
D_t	diffusion coefficient of oxygen in tissue ($cm^2\ s^{-1}$)
D_w	diffusion coefficient of oxygen in seawater ($cm^2\ s^{-1}$)
G_{pore}	conductance through single pore ($\mu mol\ s^{-1}\ kPa^{-1}$)
J_a	oxygen flux through pores across whole body ($\mu mol\ s^{-1}$)
J_{pore}	oxygen flux through a single pore ($\mu mol\ s^{-1}$)
k	constant, RT/D
k_c	k for diffusion coefficient of oxygen in cuticle, RT/D_c (cm kPa s μmol^{-1})
k_t	k for diffusion coefficient of oxygen in muscle tissue, RT/D_t (cm kPa s μmol^{-1})
k_w	k for diffusion coefficient of oxygen in seawater, RT/D_w (cm kPa s μmol^{-1})
l_c	thickness of segment of cuticle above pore (cm)
l_p	thickness of segment within pore (cm)
M	body mass
OLS	ordinary least squares regression
PD	pore density (pores cm^{-2})
PGLS	phylogenetic least squares regression
R	gas constant (cm^3 kPa $\mu mol^{-1}\ K^{-1}$)
R_{bottom}	boundary layer resistance at bottom of pore (kPa s μmol^{-1})
$R_{cuticle}$	resistance of thin piece of cuticle at top of pore (kPa s μmol^{-1})
R_{seg}	resistance of each segment within pore (kPa s μmol^{-1})
R_{top}	boundary layer resistance at top of pore (kPa s μmol^{-1})
R_{tot}	total summed resistance (kPa s μmol^{-1})
S_3	surface area of whole animal based on 3D shape (cm^2)
T	temperature (K)
V_{pore}	pore volume across whole animal (cm^3)
x	cuticle thickness or pore length (cm)
ΔP_{O_2}	oxygen gradient (kPa)

morphologically and chemically similar to the cuticles of insects and other arthropods (Davenport et al., 1987; Nentwig, 1987). The thickness of sea spider cuticle ranges from 20 to 150 µm, depending on body size (Lane et al., 2017), which is similar to observed thicknesses of insect cuticle (1 to more than 200 µm) (Vincent and Wegst, 2004) and slightly thicker than *Limulus* gill cuticle (3–10 µm) (Henry et al., 1996). Sea spiders, however, have unsclerotized and non-calcified cuticle and a microstructure that resembles the thin cuticle of the gills of *Limulus* and Malacostraca (Fahrenbach, 1994). These observations suggest that even non-porous sea spider cuticle may support high rates of oxygen diffusion. Therefore, sea spider cuticle may support relatively high diffusion coefficients of oxygen or, at least in small sea spider species, it may be thin enough to permit adequate direct diffusion of oxygen even through chitin, as has been observed in many aquatic insects (Weis-Fogh, 1964; Eriksen, 1986; Kehl and Dettner, 2009; Seymour and Matthews, 2013).

Finally, there is an intermediate scenario: each of the two pathways, pores and cuticle, supports some flux. If so, then a third hypothesis is that their relative importance changes in a size-dependent way, where smaller species with relatively thin cuticle take up oxygen directly across the cuticle and through pores while larger species take up oxygen only through pores.

To determine whether pores permit most or all of the inward flux across a range of taxa and body sizes, we measured the density and size of pores and estimated the diffusive fluxes of oxygen across sea spider cuticle. Diffusive fluxes were estimated using a mathematical model based on Fick's law (Fick, 1855; Tøien et al., 1988) that incorporated the shape of the pores and the oxygen gradient between the external and internal environments. This model allowed us to quantitatively estimate the rates of flux across individual pores, which, along with estimates of pore density, we scaled up to whole-animal fluxes of oxygen. We then compared the scaling of oxygen flux to the scaling of metabolic rate, to test the following three hypotheses (Fig. 1). (1) If pores facilitate most of the oxygen movement, then the total flux attributable to pores should closely match metabolic demand across a range of taxa and body sizes. (2) If the pores do not facilitate oxygen diffusion, then the total flux through pores should be lower than that of metabolic demand across a range of taxa and body sizes. (3) If the relative importance of pores varies in a size-dependent way, then small individuals with thin cuticles may obtain sufficient oxygen directly across the cuticle, but large individuals with relatively thick cuticles may obtain larger fractions through their pores.

MATERIALS AND METHODS

We collected sea spiders while SCUBA diving at sites in McMurdo Sound, Antarctica, in 2015 and 2016. Animals were brought to Crary Lab, McMurdo Station, and kept in seawater tables at −1 to 0°C (ambient seawater temperature ∼−1.8°C). Individuals were used within 2 weeks of collection. We collected data from 10 different species of sea spiders in five different families [Ammotheidae: *Ammothea glacialis* (Hodgson 1907), *Ammothea longispina* Gordon 1932, *Ammothea* sp.; Colossendeidae: *Colossendeis hoeki* Gordon 1944, *Colossendeis megalonyx* Hoek 1881, *Colossendeis scotti* Calman 1915; Nymphonidae: *Nymphon australe* Hodgson 1902, *Pentanymphon antarcticum* Hodgson 1904; Pallenopsidae:

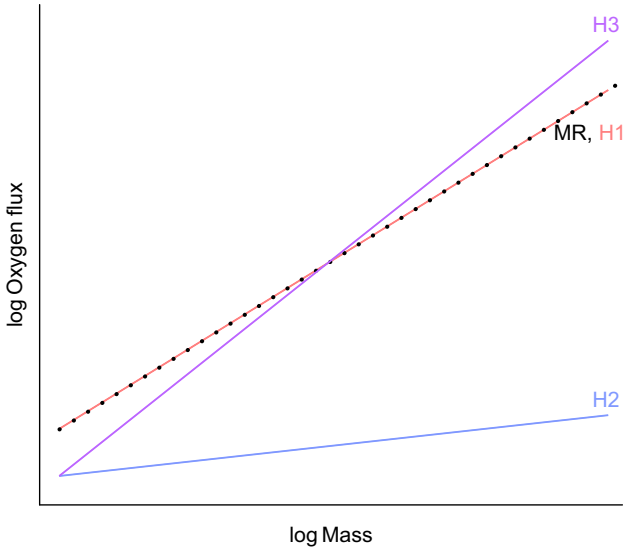

Fig. 1. Hypothesized scaling of measured metabolic rate and modeled rates of oxygen flux across pores. Metabolic rate (MR; dotted line) was taken from Lane et al. (2017). Hypothesis 1 (H1; red line): if pores facilitate most of the oxygen movement, then the total flux attributable to pores should closely match metabolic demand across a range of taxa and body sizes. Hypothesis 2 (H2; blue line): if the pores do not facilitate oxygen diffusion, then the total flux through pores should be lower than metabolic demand across a range of taxa and body sizes. Hypothesis 3 (H3; purple line): if the relative importance of pores varies in a size-dependent way, then small individuals with thin cuticles may obtain sufficient oxygen directly across the cuticle, but large individuals with relatively thick cuticles may obtain larger fractions through their pores.

Journal of Experimental Biology (2018) 221, jeb177568. doi:10.1242/jeb.177568

Pallenopsis patagonica (Hoek 1881); Pycnogonidae: *Pycnogonum gaini* Bouvier 1910]. Because we do not know the age of the animals or time since last molt, the animals used in this study were chosen without bias to cuticle condition to try and minimize any variation in cuticle condition based on age or time since last molt.

Morphological measurements

We weighed and photographed each individual. Each individual was blotted dry, to remove excess water, and then weighed on a microbalance (±0.001 g). Photographs were taken of the dorsal side, with the animal placed flat with its legs fully extended, using a Nikon D7100 digital camera (Nikon Inc., Melville, NY, USA) attached to a tripod. Surface area was estimated in ImageJ (v1.49, http://imagej.nih.gov/ij/) by tracing around the individual and multiplying by two. To account for the three-dimensional shape of the animal, we treated the body of a sea spider as an open cylinder with a calculated surface area of $S_3=2\pi rL$, where r and L are the radius and length of a leg segment, versus the surface area of a two-dimensional rectangle (S_2) of the same diameter and length ($S_2=2\times 2rL$). These two estimates of surface area are related by the expression $S_3/S_2=\pi/2$, and so $S_3=1.57\times S_2$, where S_2 was the surface area found using ImageJ.

To measure cuticle thickness, or pore length (x, cm), we prepared multiple thin sections (<1 mm each) of a single femur per individual using a razor blade. The thin sections were then mounted under a compound microscope and imaged (Zeiss Axioscope, Zeiss International, Oberkochen, Germany). From those images, we extracted cuticle thickness, which closely approximates pore length. Values were averaged per individual and then per species. Images of each cross-section (e.g. Fig. 2A,C,E,G,I) were taken using a camera mounted on a compound microscope and then analyzed in ImageJ.

We estimated pore density by taking multiple longitudinal sections of a single femur from each animal using a razor blade. Longitudinal images (e.g. Fig. 2B,D,F,H,J) were taken using a camera mounted on a compound microscope (Zeiss Axioscope). In ImageJ, pore density (PD, pores cm^{-2}) was calculated as the total number of pores in a measured area, which were counted and averaged per individual and then per species. To calculate pore volume (V_{pore}, cm^3), the total volume of the cuticle that is porous, we calculated the average volume of a single pore and then multiplied it by the total number of pores for each animal. The total number of pores was estimated by taking pore density (PD) and multiplying it by the surface area (S_3). As with cuticle thickness above, these values were averaged per species.

The above traits were measured in the femur of 10 different species. To determine whether cuticle and pore structure varied by leg segment, however, we also used the same methods to measure these traits on the 1st and 2nd tibias of three of those species: *Ammothea glacialis* (N=8), *Colossendeis megalonyx* (N=8) and *Nymphon australe* (N=8).

Oxygen gradient

Internal oxygen levels were measured within a single femur from each individual sea spider (n=46, 2–8 of each species) using a 100 µm tip Clark-style oxygen electrode (Unisense, Aarhus, Denmark) positioned using a micromanipulator. The leg was removed underwater at the proximal end of the third coxa, and the electrode tip was immediately advanced into the center of the femur. Each measurement took place within a water-jacketed glass platform. Seawater temperature was maintained at −1°C using a recirculating water bath. We also measured external oxygen levels 1 cm away from the leg segment. The electrode was connected to a

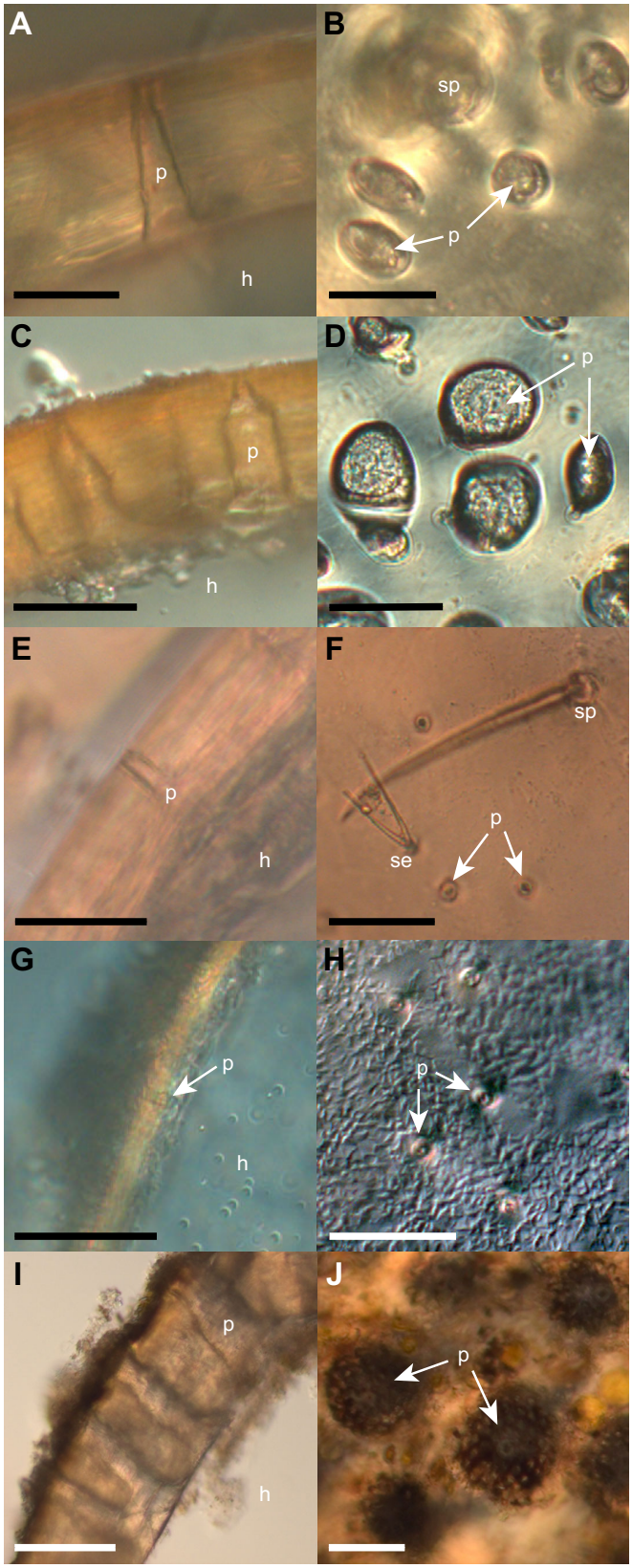

Fig. 2. Pore structure for one representative of each sea spider family in the study. Images on left side are from cross-sections and those on the right side are from longitudinal sections. (A,B) Ammotheidae, (C,D) Colossendeidae, (E,F) Nymphonidae, (G,H) Pallenopsidae, (I,J) Pycnogonidae. p, pore; h, hemocoel; sp, cuticular spines; se, cuticular setae. Scale bar: 50 µm in A–F, H and J; 25 µm in G; 100 µm in I.

Journal of Experimental Biology (2018) 221, jeb177568. doi:10.1242/jeb.177568

picoammeter (PA2000, Unisense), and data were recorded onto a computer running Expedata (v1.8.4, Sable Systems, North Las Vegas, NV, USA). Prior to each measurement, the electrode was calibrated in N_2 and air-saturated seawater at the measurement temperature (~−1°C). Internal P_{O_2} was then subtracted from external P_{O_2} to estimate the transcuticular oxygen gradient for each animal.

Oxygen consumption

We used data on oxygen consumption from Lane et al. (2017), which was obtained using closed-system respirometry. See Lane et al. (2017) for methods and data values.

Model of oxygen flux through pores

We estimated resistance to oxygen across the cuticular pores following the approach of Tøien et al. (1988), who analyzed diffusive resistance of bird eggshells using Fick's first law (Fick, 1855). We made 20 cross-sectional measurements across a single pore from each individual (Fig. 3). These measurements were made in at least three pores from each individual and then the estimated resistances were averaged. We used ImageJ to perform a segment analysis of pore morphology. Pore shape can vary substantially within an individual (e.g. Fig. 2C,I). For this analysis, however, we measured only pores that had the most common pore shape (shape shared by at least 65% of total pores per species) for each given species (e.g. identified with 'p' in Fig. 2A,C,E,G,I). We calculated resistance for a given cross-sectional segment using Fick's law:

$$R_{\text{seg}} = k \times \frac{l_{\text{p}}}{A_n}, \quad (1)$$

where R_{seg} is the resistance of each segment within the pore in kPa s μmol^{-1} (Fig. 3), l_{p} is the thickness of each cross-sectional segment in cm and A_n is the cross-sectional area of each segment in cm^2. k is a constant equal to $R{\times}T/D$ in cm kPa s μmol^{-1}, where R is the gas constant in cm^3 kPa μmol^{-1} K^{-1}, T is temperature in K, and D is the diffusion coefficient of oxygen in the body fluid within the pores in cm^2 s^{-1}. Because we did not know the diffusion coefficient of oxygen in the fluid within the pores, we bracketed our results by running two separate models with different estimates of the oxygen diffusion coefficient. One model was run by calculating k using the diffusion coefficient of oxygen in seawater ($9.86{\times}10^{-6}$ cm^2 s^{-1}) at the experimental temperature (~0°C). This model used k_{w} in place of k to calculate resistance of each cross-sectional segment (R_{seg}, Eqn 1). The second model assumed that the pores are filled with muscle tissue. Although pores likely do not contain muscle, the diffusion coefficients of oxygen in muscle are relatively well known and provide a lower limit for possible diffusion coefficients in our system. For this model, we set k as k_{t} for calculating resistance at each cross-sectional segment (R_{seg}, Eqn 1). k_{t} was calculated using the diffusion coefficient of oxygen in muscle tissue ($3.95{\times}10^{-6}$ cm^2 s^{-1}). We estimated the diffusion coefficient of oxygen through muscle tissue based on Krogh (1919) and Davenport et al. (1987), who estimated that the diffusion coefficient of oxygen in muscle tissue is approximately 40% of that in seawater.

All studied species had a small layer of cuticle separating the top of the pore from the external environment. We estimated the resistance of this thin piece of cuticle as:

$$R_{\text{cuticle}} = k_{\text{c}} \times \frac{l_{\text{c}}}{A_{\text{c}}}, \quad (2)$$

where k_{c} is the constant k described above calculated using the diffusion coefficient of oxygen in chitin. This diffusion coefficient was also estimated based on Krogh (1919), where he calculated that the diffusion coefficient of oxygen through chitin is approximately 4% that of seawater ($3.95{\times}10^{-7}$ cm^2 s^{-1}). l_{c} is the thickness of the cuticle layer (measured in ImageJ) and A_{c} is the cross-sectional area of the cuticle directly above the pore.

Like Tøien et al. (1988), we also included boundary layer resistance at the top and bottom of the pore (R_{top} and R_{bottom}, respectively; Fig. 2) using Stefan's law (Meidner and Mansfield, 1968), as shown for R_{top}:

$$R_{\text{top}} = k_{\text{w}} \times \frac{1}{2 \times d_{\text{c}}}, \quad (3)$$

where d_{c} is the diameter of the top of the pore (top cross-sectional measurement; Fig. 3). R_{bottom} was calculated similarly, except it used the constant k_{w} or k_{t} (depending on the model), and d_{20} in place of d_{c}, which was the diameter of the bottom of the pore. We estimated total resistance (R_{tot}) by summing the resistances for all the middle segments (R_{cuticle} and R_{seg}) and the boundary layer resistances (R_{top} and R_{bottom}) (Fig. 3). From R_{tot}, we calculated

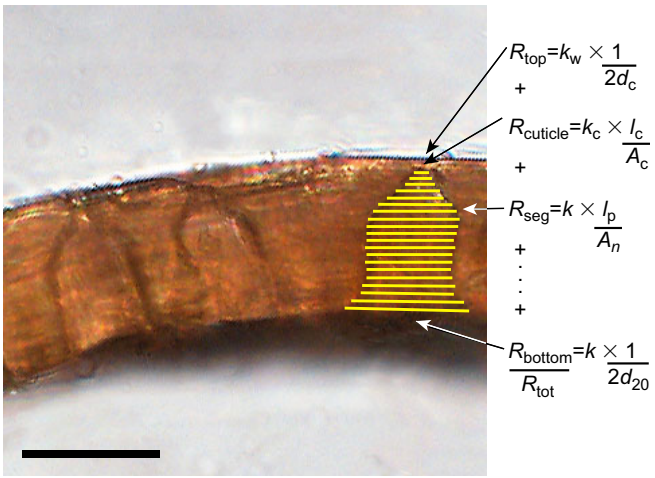

Fig. 3. Oxygen flux through cuticular pores. Diagram of pore divided into 20 equally separated segments (yellow lines). Resistance was calculated as the sum of the resistances for all 20 segments and the layer of cuticle immediately above the pore (Tøien et al., 1988). R_{top} (kPa s μmol^{-1}), which represents boundary layer resistance at the top of the pore, is inversely proportional to two times the segment diameter immediately below the layer of cuticle (d_{c}, cm). Constant k_{w} (cm kPa s μmol^{-1}) was calculated based on the oxygen diffusion coefficient through seawater. R_{bottom}, conversely, represents the boundary layer resistance at the bottom of the pore and is inversely proportional to two times the segment diameter at the bottom of the pore (d_{20}) multiplied by k, which was calculated based on the diffusion coefficient of oxygen through seawater or muscle tissue. R_{cuticle} represents the resistance through the portion of cuticle above the pore. l_{c} (cm) is the thickness of the cuticular cap above the pore and was divided by the cross-sectional area (A_{c}, cm^2) of the first segment, assuming the segment is circular. The following middle segment resistances (R_{seg}) were calculated using the thickness of each segment through the pore (l_{p}), which was the same for each segment, divided by the cross-sectional area (A_n). A_n was calculated by measuring the segmental pore diameter (d_n) and assuming each segment is circular. The constant k was calculated as $k{=}RT/D$ (cm kPa s μmol^{-1}), where R is the gas constant, T is temperature and D is the diffusion coefficient of the material (water, cuticle or tissue). See Materials and methods for more details. Scale bar: 50 μm.

conductance through a single pore (G_{pore}, μmol s^{-1} kPa^{-1}):

$$G_{pore} = \frac{1}{R_{tot}}, \quad (4)$$

where conductance is a measure of how fast oxygen moves across a material given a difference in partial pressure (Dejours, 1981).

The diffusive oxygen flux through a single pore (J_{pore}, μmol s^{-1}) was then calculated using Fick's first law (Dejours, 1981):

$$J_{pore} = G_{pore} \times \Delta P_{O_2}, \quad (5)$$

where ΔP_{O_2} is the oxygen gradient in kPa, and J_{pore} is the number of moles of oxygen moving across a single pore per unit time. We then scaled this up to the whole body (J_a) by multiplying the diffusive oxygen flux across a single pore by the density of pores (PD, pores cm^{-2}) and then the total calculated surface area of the animal (S_3, cm^2):

$$J_a = J_{pore} \times (PD \times S_3). \quad (6)$$

We then compared whole-body oxygen flux for a given species with the species' oxygen consumption (Lane et al., 2017) to determine how well the total diffusive oxygen flux through the pores matched whole-animal oxygen uptake.

Because most oxygen uptake occurs across the sea spider's legs (Davenport et al., 1987), we focused our analyses on the pore morphology and physiology of the major leg segments. To determine whether there was any variation among segments within individuals and species, we estimated oxygen conductance through an average pore on the femur, first tibia and second tibia of three species [*Ammothea glacialis* (n=8), *Colossendeis megalonyx* (n=8) and *Nymphon austral* (n=3–4)] following the methods described above. Using a linear mixed effects model, with individual as a random factor, we did not find any differences between leg segments for any of the three species for any of the measured variables (Tables S1 and S3). We therefore used pore characteristics from just the femur of each species, which were extrapolated to the whole animal using Eqn 6.

Statistical analyses

For all scaling analyses, we measured body mass, pore diameter, pore length, pore density, pore volume, oxygen flux and oxygen consumption in 10 different species (from five different families) of sea spiders (Tables S4 and S5). To compare how those traits changed with body size, we $\log_{10}$-transformed the data and fitted ordinary least squares regressions (OLS). For each trait, we took the average measurements from 2–8 individuals, which varied depending on the trait. However, for several species (*Ammothea* sp., *Colossendeis hoeki*, *Pallenopsis patagonica*, *Pentanymphon antarcticum* and *Pycnogonum gaini*), we collected data on pore density from only one individual.

To account for potential phylogenetic effects on traits, we also conducted phylogenetic least squares regressions (PGLS) on the data following the procedures of Lane et al. (2017). We constructed trees using mitochondrial cytochrome *c* oxidase (CO1) sequences collected from our samples and then conducted PGLS analyses using: (1) an unconstrained phylogeny built from our CO1 data (PGLS-mtCO1) and (2) a constrained phylogeny following the tree topology of Arango and Wheeler (2007) in which branch lengths were free to vary based on our CO1 data (PGLS-var. brlens). The tree from Arango and Wheeler (2007) was constructed using three nuclear and three mitochondrial genes from 63 different species, representing all 9 sea spider families. We also created a third tree using the constrained topology above but with equal branch lengths (PGLS-equal brlens). As in the OLS models described above, we used species averages and $\log_{10}$-transformed the data prior to running each PGLS model.

We then used Pagel's lambda (Pagel, 1999) to test for phylogenetic signal. Only two variables showed a significant phylogenetic signal (pore diameter and pore density; Table S2). In the two cases where we detected a phylogenetic signal, the PGLS model results are reported in the text and figures (only PGLS-equal brlens are reported, for brevity); otherwise, the OLS results were reported (see Table 1 and Table S2 for full results).

All statistical analyses were conducted in R (v3.3.0, http://www.R-project.org/) and the PGLS models were conducted using the R package 'ape' (v3.5) (Pagel, 1992). Data are reported as means±s.e.m.

RESULTS

Interspecific variation in pore morphology

A phylogenetic signal was detected for pore diameter (d, μm), pore density (PD, pores cm^{-2}) and pore volume (V_{pore}, cm^3) with the PGLS-equal brlens model (Table S2), so the PGLS results are presented here, while no signal was detected for pore length (x, μm) (Table S2), so the OLS results are presented here (see Table 1 for regression summary of all models). Pore length and pore diameter both increased with body size (Fig. 4A,B, respectively, Table 1). The relationship between pore length (x, μm) and body mass (M, g) is $x=-2.30\times M^{0.37}$. For pore diameter (d, μm) the relationship with body size is $d=1.17\times M^{0.30}$. Pore density decreased slightly with increasing body size as $PD=4.32\times M^{-0.23}$ (Fig. 4C). *Pycnogonum gaini*, which had substantially fewer pores per square centimeter than expected for its body size (over one order of magnitude lower), was treated as an outlier and was not included in the pore density analysis. Total pore volume of the entire cuticle (V_{pore}, cm^3) increased with increasing body size as $V_{pore}=-2.56\times M^{1.35}$ (Fig. 4D).

Oxygen flux and oxygen consumption

We did not observe significant differences when diffusive oxygen flux was estimated using an assumed diffusion coefficient for water or tissue (Table 1). Therefore, for brevity, only the tissue model is described here.

Diffusive oxygen flux across the cuticular pores and oxygen consumption both increased with body size (Fig. 5, Table 1). The relationship between oxygen flux (J_a, μmol s^{-1}), using the tissue model, and body size is $J_a=-4.13\times M^{1.01}$. The relationship between oxygen consumption (OC, μmol s^{-1}) and body size is $OC=-3.96\times M^{0.80}$. Furthermore, the regression coefficient for slope and intercept did not vary between oxygen flux and oxygen consumption based on overlapping confidence intervals (Table 1).

DISCUSSION

Although we cannot formally disprove hypothesis 2, that gas exchange occurs across solid cuticle, our data support hypothesis 1, that sea spiders take up oxygen primarily via cuticular pores. Broadly speaking, there was a close match between the scaling of known rates of oxygen uptake (based on our measurements of metabolic rate; Lane et al., 2017) and the scaling of calculated rates of oxygen flux via pores. Those fluxes match closely over two orders of magnitude in body size. Nevertheless, our data also suggest some size dependence of the relative contribution of pore-based fluxes (H3, Fig. 1). In large-bodied species, estimated pore-based fluxes were higher than measured metabolic rates, whereas in

Journal of Experimental Biology (2018) 221, jeb177568. doi:10.1242/jeb.177568

Table 1. Summary of OLS and PGLS regression analyses

Model	*N*	*a*	95% CI	*P*	*b*	95% CI	*P*	R^2
x vs *M*								
OLS	10	−2.30	−2.53, −2.06	<0.001	0.37	0.00, 0.74	0.049	0.33
PGLS-mtCO1	10	−2.44	−2.93, −1.94	<0.001	0.18	−0.19, 0.56	0.286	
PGLS-var. brlens	10	−2.35	−2.74, −1.96	<0.001	0.20	−0.20, 0.59	0.281	
PGLS-equal brlens	10	−2.28	−2.74, −1.82	<0.001	0.23	−0.15, 0.60	0.196	
d vs *M*								
OLS	10	1.14	0.93, 1.35	<0.001	0.42	0.08, 0.76	0.020	0.45
PGLS-mtCO1	10	1.06	0.63, 1.49	<0.001	0.29	−0.03, 0.61	0.069	
PGLS-var. brlens	10	1.12	0.80, 1.44	<0.001	0.30	−0.02, 0.63	0.064	
PGLS-equal brlens	10	1.17	0.82, 1.52	<0.001	0.30	0.02, 0.58	0.038	
PD vs *M*								
OLS	9	4.33	4.25, 4.41	<0.001	−0.12	−0.23, 0.00	0.053	0.35
PGLS-mtCO1	9	4.31	4.14, 4.48	<0.001	−0.23	−0.35, −0.11	0.003	
PGLS-var. brlens	9	4.31	4.18, 4.44	<0.001	−0.23	−0.35, −0.11	0.003	
PGLS-equal brlens	9	4.32	4.17, 4.48	<0.001	−0.23	−0.35, −0.11	0.003	
V_{pore} vs *M*								
OLS	10	−2.51	−3.03, −1.99	<0.001	1.79	0.97, 2.61	0.001	0.73
PGLS-mtCO1	10	−2.89	−4.04, −1.75	<0.001	1.25	0.40, 2.11	0.010	
PGLS-var. brlens	10	−2.72	−3.60, −1.84	<0.001	1.28	0.39, 2.17	0.010	
PGLS-equal brlens	10	−2.56	−3.54, −1.57	<0.001	1.35	0.55, 2.14	0.005	
J_a vs *M**								
OLS	10	−3.84	−4.09, −3.60	<0.001	0.99	0.60, 1.37	<0.001	0.79
PGLS-mtCO1	10	−3.80	−4.38, −3.22	<0.001	1.04	0.60, 1.48	<0.001	
PGLS-var. brlens	10	−3.86	−4.31, −3.41	<0.001	1.04	0.59, 1.48	<0.001	
PGLS-equal brlens	10	−3.89	−4.46, −3.32	<0.001	1.03	0.56, 1.49	<0.001	
J_a vs *M*‡								
OLS	10	−3.94	−4.17, −3.70	<0.001	1.01	0.64, 1.39	<0.001	0.81
PGLS-mtCO1	10	−3.91	−4.48, −3.34	<0.001	1.01	0.59, 1.44	<0.001	
PGLS-var. brlens	10	−3.96	−4.40, −3.53	<0.001	1.01	0.57, 1.44	<0.001	
PGLS-equal brlens	10	−3.99	−4.55, −3.43	<0.001	1.00	0.55, 1.45	0.001	
OC vs *M*								
OLS	10	−3.96	−4.15, −3.77	<0.001	0.80	0.52, 1.08	<0.001	0.83
PGLS-mtCO1	10	−4.03	−4.47, 3.59	<0.001	0.77	0.46, 1.07	<0.001	
PGLS-var. brlens	10	−4.01	−4.34, −3.69	<0.001	0.77	0.46, 1.07	<0.001	
PGLS-equal brlens	10	−3.99	−4.39, −3.60	<0.001	0.75	0.47, 1.04	<0.001	

N, number of species used in each analysis. Regression coefficients: intercept (*a*) and scaling exponent (*b*).
x, pore length (cm); *M*, body mass (g); *d*, pore diameter (cm); PD, pore density (pores cm^{-2}); V_{pore}, pore volume (cm^3); J_a, whole-animal flux (μmol s^{-1}); OC, oxygen consumption (μmol s^{-1}); OLS, ordinary least squares regressions; PGLS, phylogenetic least squares regressions. PGLS models are as follows: mtCO1, tree built with unconstrained topology; var. brlens, tree with variable branch lengths; equal brlens, same tree topology but with all branch lengths set to 1. Individual oxygen consumption rates were taken from Lane et al. (2017).
*Oxygen flux calculated using the diffusion coefficient of seawater (D_w). ‡Oxygen flux calculated using the diffusion coefficient of muscle tissue (D_t).

small-bodied species they were lower (Fig. 4). This pattern suggests that large-bodied species rely more exclusively on pore-based fluxes of oxygen. The broad confidence intervals in our data (Table 1) preclude distinguishing hypotheses 1 and 3 more quantitatively.

The size dependence of oxygen uptake via pores emerges from the scaling of pore morphology. Larger species have thicker cuticle (as described by pore length), which decreases flux by increasing the distance that oxygen must move. Cuticle thickness and pore diameter scaled approximately as expected for geometric similarity (b=0.37 and b=0.30, respectively). Pore density decreased slightly with increasing body size (b=−0.23). Pore volume, however, scaled with a larger coefficient (b=1.35) than expected for geometric similarity (b=1.00; Schmidt-Nielsen, 1984). This means that to offset the decrease in flux associated with thicker cuticle, larger species have wider pores, which results in greater total pore volume.

Rather than possess high pore density, one of the species in our study – *Pycnogonum gaini* – maintains adequate diffusive oxygen flux with relatively few but large pores. For its body size, *Pycnogonum gaini* (Fig. 2E) has substantially fewer pores per square area than expected, which would convey relatively low oxygen flux. Nevertheless, it meets its required diffusive fluxes of oxygen by also having much wider pores than expected for its body size.

The boundary layer resistance above and below the pores conferred little resistance to oxygen movement (Table S6). Therefore, flow conditions across the outer cuticle or within the hemolymph likely have little effect on total oxygen flux. Conversely, in most species, the cuticular cap conferred the greatest resistance to oxygen diffusion. For example, in the three *Colossendeis* species, resistance across the cuticular cap accounted for over 80% of the total resistance. The thickness of this cap can play a large role in restricting oxygen flux. Colonizing organisms, such as bryozoans, could increase the functional thickness of the cuticle and greatly decrease oxygen flux. We are currently testing the effects of different colonizing organisms on sea spider gas exchange.

To calculate resistance at the top and bottom of each pore, we used Stefan's law. This is appropriate when the diffusing molecule enters or leaves the pore from a concentration gradient distributed hemispherically around the pore opening. This is possible only if the pore openings are spaced far enough apart – otherwise, the hemispherical concentration gradients interfere with one another, which has the effect of raising the total resistance (Brown and Escombe, 1900; Ting and Loomis, 1963). In general, Stefan's law is thought to hold if pore openings are spaced more than 10 diameters apart. In our study, pore openings on the external cuticle met this

Journal of Experimental Biology (2018) 221, jeb177568. doi:10.1242/jeb.177568

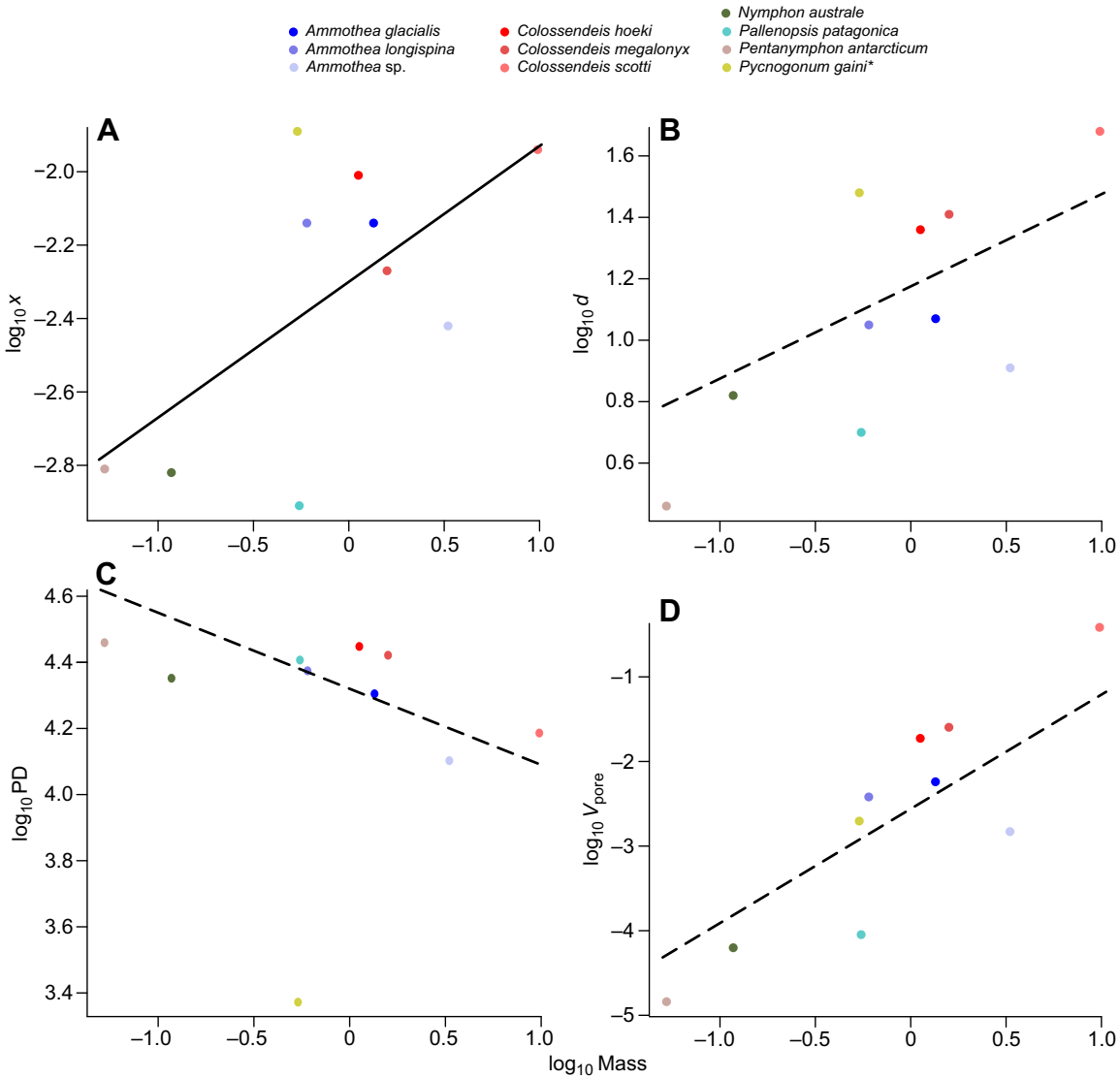

Fig. 4. Regression lines for scaling relationships to body mass. (A) Pore length (*x*, measured as cuticle thickness in μm; *n*=10), (B) pore diameter (*d*, μm; *n*=10), (C) pore density (PD, pores cm^{-2}; *n*=9) and (D) pore volume across the entire cuticle (V_{pore}, cm^3; *n*=10). Body mass was measured in g. In A, the line indicates the fit using ordinary least squares regression (OLS); in B–D, lines indicate the fit using phylogenetic least squares regressions (PGLS) with equal branch length. See Results for details. See Table 1 for regression coefficients. **Pycnogonum gaini* appears to be an outlier and was not used in the pore density regression.

assumption (data not shown). Conversely, pore openings on the internal side of the cuticle generally were closer than 10 diameters from one another, thus violating the Stefan assumption. Theoretically, this raises the total resistance provided by the internal layers of hemolymph. We decided, however, to ignore this problem – both because the calculated internal resistances are of the order of 1% of the total resistance, and because agitation of the hemolymph by gut peristalsis (Woods et al., 2017) probably reduces this resistance anyway.

The presence of pores in the cuticle likely presents a functional trade-off between gas exchange and structural support: a greater total pore volume supports greater fluxes of oxygen but likely also weakens the cuticle. Alternatively, thicker cuticle provides greater strength, but it reduces the rate of diffusive oxygen flux by lengthening the pores. While many studies have discussed the relationship between shell thickness, shell material composition and structural support in eggshells (Ar et al., 1979; Board and Scott, 1980; Board, 1980), few have tested the relationship between structural support and porosity. Tyler (1955) discussed whether the distribution of pores in avian egg shells, ∼2 pores per square millimeter, helps reduce the number of weak areas in an egg shell as areas of greater pore density would be weaker and act as sites for crack propagation. The relationship between structural support and pore shape has also been studied in vertebrate bones and engineered materials. In vertebrate bones, increasing porosity lowers fracture strength, the ability of a material to withstand breaking, because pores reduce the load-bearing area of the bone (Yeni et al., 1997). In metallic glass, an amorphous metal used in electronics and medical devices, and ceramic microsieves, material used in microfiltration, the diameter of the pore affects material strength; wider pores yield weaker material strength because the edge of the pore is the weakest point, so pores with larger diameters will be weaker than those with smaller diameters (Gao et al., 2016; Kuiper et al., 2002).

The structure of sea spider cuticle may therefore present an evolutionary compromise to minimize strength reduction while

Journal of Experimental Biology (2018) 221, jeb177568. doi:10.1242/jeb.177568

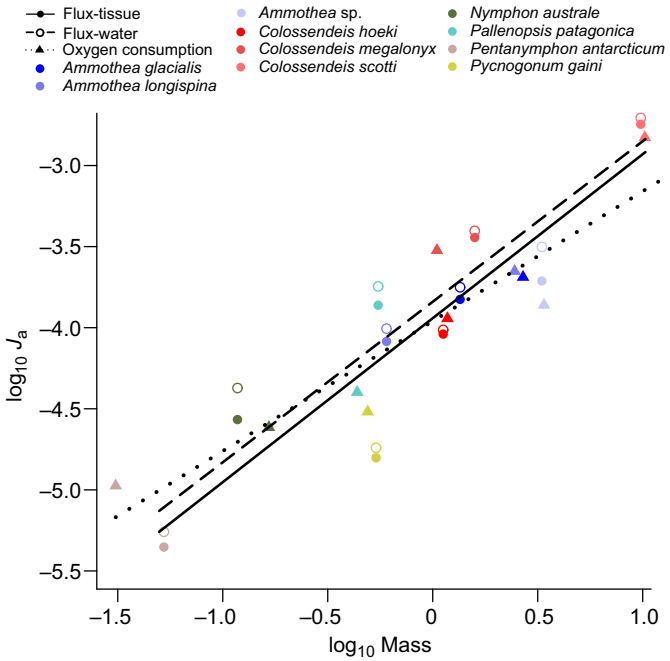

Fig. 5. Oxygen flux and consumption. Regression lines comparing total diffusive oxygen flux (J_a) through pores using the tissue-diffusion model, the water-diffusion model and oxygen consumption to body mass. Oxygen flux was measured in μmol s^{-1} and body mass in g. Regression lines were calculated based on OLS models. *N*=10. Oxygen consumption rates were taken from Lane et al. (2017). See Table 1 for regression coefficients.

maintaining sufficient oxygen flux, as we have hypothesized recently (Lane et al., 2017). In an absolute sense, large sea spiders have thicker cuticle, which provides greater strength but also long distances over which oxygen must diffuse. Large species, therefore, must have larger average diameter pores to offset the resistance to oxygen flux arising from these long distances, which may weaken the cuticle. The species of *Colossendeis* and *Ammothea* are the largest-bodied individuals in our analyses, and they have many conical pores, with the small aperture near the surface of the cuticle. This pore design may allow these species to grow to relatively large sizes by minimizing the structural weakness associated with pores, because conical pores concentrate chitinous material away from the central axis and therefore offer greater polar moments of area (Vogel, 2013) relative to the same pore areas distributed by cylinder pores. We are presently testing the structural integrity of sea spider cuticles with different pore shapes and densities.

In conclusion, sea spider cuticle is not solid but, rather, contains many pores (Fahrenbach, 1994; Davenport et al., 1987). The volume and density of pores both scale with body size to allow sufficient oxygen into the body to meet the sea spider's metabolic demands, especially for larger-bodied species. Future studies should examine sea spiders from different environments, such as those living in temperate or tropical locations or those living in the intertidal zone, to see whether pore structure changes with temperature or the likelihood of strong external forces. For instance, because higher temperatures stimulate metabolic rate more than they do rates of diffusive flux (Woods, 1999; Verberk et al., 2011), we predict that, for their small body sizes, tropical species will have higher conductance cuticles, which could be achieved by thinner or more porous cuticle. The trade-off discussed above may be more acute for warm-water species, as those living in the intertidal zone and other areas with higher current may be more at risk from external forces (e.g. tide cycles, current surges) and may need proportionately thicker cuticle with fewer pores to prevent structural damage.

Acknowledgements

We thank the directors and staff at McMurdo Station for field and technical support. Also, special thanks to Rob Robbins, Steve Rupp and Tim Dwyer for SCUBA support. We also thank Peter Marko, Michael Wallstrom, Floyd Reed, Sachie Etherington and the entire class of BIOL 375L from fall 2016 at the University of Hawai'i at Mānoa for their contributions to the barcoding effort.

Competing interests

The authors declare no competing or financial interests.

Author contributions

Conceptualization: S.J.L., A.L.M., B.W.T., H.A.W.; Methodology: S.J.L., A.L.M., H.A.W.; Software: S.J.L., H.A.W.; Validation: S.J.L., A.L.M., B.W.T., H.A.W.; Formal analysis: S.J.L., H.A.W.; Investigation: S.J.L., C.M.S., H.A.W.; Resources: S.J.L., A.L.M., C.M.S., B.W.T., H.A.W.; Writing - original draft: S.J.L., A.L.M., B.W.T., H.A.W.; Writing - review & editing: S.J.L., A.L.M., C.M.S., B.W.T., H.A.W.; Visualization: S.J.L., A.L.M.; Supervision: A.L.M., B.W.T., H.A.W.; Project administration: A.L.M., B.W.T., H.A.W.; Funding acquisition: A.L.M., B.W.T., H.A.W.

Funding

This work was funded by the US National Science Foundation Division of Polar Programs (PLR-1341485 to H.A.W. and B.W.T., PLR-1341476 to A.L.M.).

Supplementary information

Supplementary information available online at
http://jeb.biologists.org/lookup/doi/10.1242/jeb.177568.supplemental

References

Ar, A., Rahn, H. and Paganelli, C. V. (1979). The avian egg: mass and strength. *The Condor* **81**, 331-337.

Arango, C. P. and Wheeler, W. C. (2007). Phylogeny of the sea spiders (Arthropoda, Pycnogonida) based on direct optimization of six loci and morphology. *Cladistics* **23**, 255-293.

Arnaud, F. and Bamber, R. N. (1987). The biology of Pycnogonida. *Adv. Mar. Biol.* **24**, 1-96.

Board, R. G. (1980). Properties of avian egg shells and their adaptive value. *Biol. Rev.* **57**, 1-28.

Board, R. G. and Scott, V. D. (1980). Porosity of the avian eggshell. *Am. Zool.* **20**, 339-349.

Brown, H. T. and Escombe, F. (1900). Static diffusion of gases and liquids in relation to the assimilation of carbon and translocation in plants. *Philos Trans. R. Soc. Lond. B Biol. Sci.* **193**, 223-291.

Child, C. A. (1995). Antarctic and subantarctic pycnogonids. Nymphonidae, Colossendeidae, Rhynchothoracidae, Pycnogonidae, Endeidae and Callipallenidae. In *Biology of Antarctic Seas XXIV, Antarctic Research Series*, Vol. 69 (ed. S. D. Cairns), pp. 1-165. Washington, DC: American Geophysical Union.

Davenport, J., Blackstock, N., Davies, D. A. and Yarrington, M. (1987). Observations on the physiology and integumentary structure of the Antarctic pycnogonid *Decolopoda australis*. *J. Zool.* **211**, 451-465.

Dejours, P. (1981). *Principles of Comparative Respiratory Physiology*, p. 265. Amsterdam: Elsevier/North-Holland Biomedical Press.

Dell, R. K. (1972). Antarctic benthos. In *Advances in Marine Biology*, Vol. 10 (ed. F. S. Russell and M. Yonge), pp. 102-172. London: Academic Press.

Eriksen, C. H. (1986). Respiratory roles of caudal lamellae (gills) in a Lestid damselfly (Odonata:Zygoptera). *J. North. Am. Benthol. Soc.* **5**, 16-27.

Fahrenbach, W. H. (1994). Microscopic anatomy of Pycnogonida: I. cuticle, epidermis, and muscle. *J. Morph.* **222**, 33-48.

Feder, M. E. and Burggren, W. W. (1985). Skin breathing in vertebrates. *Sci. Am.* **253**, 126-142.

Fick, A. (1855). Ueber diffusion. *Ann. Phys.* **170**, 59-86.

Gao, M., Dong, J., Huan, Y., Wang, Y. T. and Wang, W.-H. (2016). Macroscopic tensile plasticity by scalarizating stress distribution in bulk metallic glass. *Sci. Rep.* **6**, 21929.

Graham, J. B. (1988). Ecological and evolutionary aspects of integumentary respiration: body size, diffusion, and the invertebrata. *Amer. Zool.* **28**, 1031-1045.

Henry, R. P., Jackson, S. A. and Mangum, C. P. (1996). Ultrastructure and transport-related enzymes of the gills and coxal gland of the horseshoe crab *Limulus Polyphemus*. *Biol. Bull.* **191**, 241-250.

Hinton, H. E. (1981). *Biology of Insect Eggs*, Vol. 1, 473 p. Elmsford, NY: Pergammon Press.

Kehl, S. and Dettner, K. (2009). Surviving submerged-setal tracheal gills for gas exchange in adult rheophilic diving beetles. *J. Morph.* **270**, 1348-1355.
Kern, M. D. and Ferguson, M. W. J. (1997). Gas permeability of American alligator eggs and its anatomical basis. *Physiol. Zool.* **70**, 530-546.
King, P. E. (1973). *Pycnogonids*, 144 p. London: Hutchinson.
Krogh, A. (1919). The rate of diffusion of gases through animal tissues, with some remarks on the coefficient of invasion. *J. Phys.* **52**, 391-408.
Kuiper, S., Brink, R., Nijdam, W., Krijnen, G. J. M. and Elwenspoek, M. C. (2002). Ceramic microsieves: influence of perforation shape and distribution on flow resistance and membrane strength. *J. Memb. Sci.* **196**, 149-157.
Lane, S. J., Shishido, C. M., Moran, A. L., Tobalske, B. W., Arango, C. P. and Woods, H. A. (2017). Upper limits to body size imposed by respiratory-structural trade-offs in Antarctic pycnogonids. *Proc. R. Soc. B* **284**, 20171779.
Meidner, H. and Mansfield, T. A. (1968). *Physiology of Stomata*. New York: McGraw Hill.
Moran, A. L. and Woods, H. A. (2012). Why might they be giants? Towards an understanding of polar gigantism. *J. Exp. Biol.* **215**, 1995-2002.
Nentwig, W. (1987). *Ecophysiology of Spiders*, 447pp. Berlin: Springer-Verlag.
Paganelli, C. V. (1980). The physics of gas exchange across the avian eggshell. *Am. Zool.* **20**, 329-338.
Pagel, M. D. (1992). A method for the analysis of comparative data. *J. Theor. Biol.* **156**, 431-442.
Pagel, M. D. (1999). Inferring the historical patterns of biological evolution. *Nature* **401**, 877-884.
Rahn, H. and Paganelli, C. V. (1990). Gas fluxes in avian eggs: driving forces and the pathway for exchange. *Comp. Biochem. Physiol. A Physiol.* **95**, 1-15.
Resh, V. H., Buchwater, D. B., Lamberti, and Eriksen, C. H. (2008). Aquatic insect respiration. *An Introduction to the Aquatic Insects of North America*, 4th edn. (ed. R. W. Merritt, K. L. Cummins and M. B. Berg), pp. 39-54. Dubuque, IA: Kendall/Hunt Pub Co.
Rokitka, M. A. and Rahn, H. (1987). Regional differences in shell conductance and pore density of avian egg eggs. *Resp. Phys.* **68**, 371-376.
Schmidt-Nielsen, K. (1984). *Scaling: Why is Animal Size so Important?* p. 241. Cambridge: Cambridge University Press.
Seymour, R. S. and Matthews, P. G. D. (2013). Physical gills in diving insects and spiders: theory and experiment. *J. Exp. Biol.* **216**, 164-170.
Ting, I. P. and Loomis, W. E. (1963). Diffusion through stomates. *Am. J. Bot.* **50**, 866-872.
Tøien, Ø., Paganelli, C. V., Rahn, H. and Johnson, R. R. (1988). Diffusive resistance of avian eggshell pores. *Resp. Phys.* **74**, 345-354.
Tyler, C. (1955). Studies on eggshells. IV. The distribution of pores in eggshells. *J. Sci. Food Agric.* **6**, 170-176.
Verberk, W. C. E. P., Bilton, D. T., Calosi, P. and Spicer, J. I. (2011). Oxygen supply in aquatic ectotherms: partial pressure and solubility together explain biodiversity and size patterns. *Ecology* **92**, 1565-1572.
Vincent, J. F. V. and Wegst, U. G. K. (2004). Design and mechanical properties of insect cuticle. *Arthropod. Struct. Dev.* **33**, 187-199.
Vogel, S. (2013). *Comparative Biomechanics: Life's Physical World*. Princeton, NJ: Princeton University Press.
Wangensteen, O. D., Wilson, D. and Rahn, H. (1971). Diffusion of gases across the shell of the hen's egg. *Resp. Phys.* **11**, 16-30.
Weibel, E. R., Taylor, C. R. and Bolis, L. (1998). *Principles of Animal Design. The Optimization and Symmorphosis Debate*, pp. 314. Cambridge: Cambridge University Press.
Weis-fogh, T. (1964). Diffusion in insect wing muscle, the most active tissue known. *J. Exp. Biol.* **41**, 229-256.
Woods, H. A. (1999). Egg-mass size and cell size: effects of temperature on oxygen distribution. *Am. Zool.* **39**, 244-252.
Woods, H. A., Bonnecaze, R. T. and Zrubek, B. (2005). Oxygen and water flux across eggshells of *Manduca sexta*. *J. Exp. Biol.* **208**, 1297-1308.
Woods, H. A., Lane, S. J., Shishido, C., Tobalske, B. W., Arango, C. P. and Moran, A. L. (2017). Respiratory gut peristalsis by sea spiders. *Curr. Biol.* **27**, R638-R639.
Yeni, Y. N., Brown, C. U., Wang, Z. and Norman, T. L. (1997). The influence of bone morphology on fracture toughness of the human femur and tibia. *Bone* **21**, 453-459.

Supplementary Information for *Cuticular gas exchange by Antarctic sea spiders*

Lane, SJ, AL Moran, CM Shishido, BW Tobalske, and HA Woods

Journal of Experimental Biology

Table S1. Intravariation of cuticle morphology and physiology between leg segments in three species of sea spiders: pore length (μm), pore diameter (μm), pore density (pores cm^{-2}), conductance_water (μmol s^{-1} kPa^{-1} $pore^{-1}$), and conductance_tissue (μmol s^{-1} kPa^{-1} $pore^{-1}$).

Variable	Species	leg segment	*N*	mean	s.e.m.	*F*	*P*
Pore length							
	Ammothea glacialis	femur	8	72.96	± 2.06	0.712	0.507
		1st tibia	8	67.20	± 2.59		
		2nd tibia	8	68.72	± 5.19		
	Colossendeis megalonyx	femur	8	53.12	± 2.10	1.883	0.189
		1st tibia	8	51.31	± 1.73		
		2nd tibia	8	54.69	± 1.41		
	Nymphon australe	femur	3	15.31	± 3.09	0.638	0.575
		1st tibia	3	20.00	± 10.00		
		2nd tibia	4	21.25	± 4.27		
Pore diameter							
	Ammothea glacialis	femur	8	12.91	± 0.40	2.192	0.149
		1st tibia	8	14.14	± 0.64		
		2nd tibia	8	13.92	± 0.53		
	Colossendeis megalonyx	femur	8	25.66	± 1.23	0.576	0.575
		1st tibia	8	24.04	± 1.80		
		2nd tibia	8	25.06	± 1.10		
	Nymphon australe	femur	3	6.56	± 1.13	1.201	0.391
		1st tibia	3	6.72	± 0.45		
		2nd tibia	4	5.67	± 0.33		
Pore density							
	Ammothea glacialis	femur	8	22062	± 944	2.241	0.143
		1st tibia	8	22553	± 924		
		2nd tibia	8	24274	± 745		
	Colossendeis megalonyx	femur	8	26384	± 1830	0.860	0.445
		1st tibia	8	26207	± 1131		
		2nd tibia	8	27509	± 1372		
	Nymphon australe	femur	8	16993	± 2175	1.168	0.340

		1st tibia	8	17032	± 1833		
		2nd tibia	8	20086	± 1038		
Conductance_water							
	Ammothea glacialis	femur	8	6.14×10^{-11}	$\pm 8.87 \times 10^{-12}$	3.654	0.053
		1st tibia	8	4.64×10^{-11}	$\pm 5.19 \times 10^{-12}$		
		2nd tibia	8	3.75×10^{-11}	$\pm 3.66 \times 10^{-12}$		
	Colossendeis megalonyx	femur	8	8.46×10^{-11}	$\pm 9.97 \times 10^{-12}$	2.110	0.158
		1st tibia	8	7.09×10^{-11}	$\pm 1.76 \times 10^{-11}$		
		2nd tibia	8	5.01×10^{-11}	$\pm 4.07 \times 10^{-12}$		
	Nymphon australe	femur	3	2.62×10^{-10}	$\pm 4.60 \times 10^{-11}$	4.264	0.102
		1st tibia	3	1.74×10^{-10}	$\pm 3.81 \times 10^{-11}$		
		2nd tibia	4	1.35×10^{-10}	$\pm 1.21 \times 10^{-11}$		
Conductance_tissue							
	Ammothea glacialis	femur	8	4.99×10^{-11}	$\pm 1.73 \times 10^{-11}$	3.596	0.055
		1st tibia	8	4.02×10^{-11}	$\pm 1.10 \times 10^{-11}$		
		2nd tibia	8	3.28×10^{-11}	$\pm 8.52 \times 10^{-12}$		
	Colossendeis megalonyx	femur	8	7.66×10^{-11}	$\pm 8.85 \times 10^{-12}$	1.988	0.174
		1st tibia	8	6.35×10^{-11}	$\pm 1.57 \times 10^{-11}$		
		2nd tibia	8	4.68×10^{-11}	$\pm 3.65 \times 10^{-12}$		
	Nymphon australe	femur	3	1.71×10^{-10}	$\pm 3.26 \times 10^{-11}$	3.455	0.134
		1st tibia	3	1.23×10^{-10}	$\pm 2.63 \times 10^{-11}$		
		2nd tibia	4	9.21×10^{-11}	$\pm 3.90 \times 10^{-12}$		

Table S2. Pagel's lambda and log likelihood scores for PGLS regression analyses.

Models	*N*	Pagel's Lambda	logL	logL0	logL P-value
Pore length (cm) *vs weight* (g)					
PGLS-mtCO1	10	1.00	-1.96	-3.60	0.070
PGLS-var. brlens	10	1.00	-1.89	-2.40	0.310
PGLS-equal brlens	10	1.00	-1.91	-3.50	0.075
Pore diameter (cm) *vs weight* (g)					
PGLS-mtCO1	10	1.00	0.10	-1.58	0.067
PGLS-var. brlens	10	1.00	0.34	-1.24	0.075
PGLS-equal brlens	10	1.00	0.67	-2.29	0.015
Pore density (pores cm^{-2}) *vs weight* (g)					
PGLS-mtCO1	9	1.00	10.21	8.21	0.045
PGLS-var. brlens	9	1.00	10.38	7.96	0.028
PGLS-equal brlens	9	1.00	9.98	6.68	0.010
Pore volume (cm^3) *vs weight* (g)					
PGLS-mtCO1	10	0.89	-10.66	-11.83	0.126

PGLS-var. brlens	10	0.68	-10.54	-11.05	0.315
PGLS-equal brlens	10	1.00	-8.43	-10.54	0.040
Whole animal flux (µmol s^{-1}) *vs weight* (g) (D = water)					
PGLS-mtCO1	10	1.00	-1.96	-2.13	0.562
PGLS-var. brlens	10	0.00	-1.58	-1.58	1.000
PGLS-equal brlens	10	1.00	-3.77	-3.78	0.869
Whole animal flux (µmol s^{-1}) *vs weight* (g) (D = tissue)					
PGLS-mtCO1	10	0.00	-1.99	-1.99	1.000
PGLS-var. brlens	10	0.00	-1.59	-1.59	1.000
PGLS-equal brlens	10	0.00	-3.33	-3.33	1.000
Oxygen consumption (µmol s^{-1}) *vs weight* (g)					
PGLS-mtCO1	10	0.55	0.69	0.50	0.548
PGLS-var. brlens	10	0.65	0.68	0.25	0.352
PGLS-equal brlens	10	1.00	0.97	0.03	0.169

Table S3. Summary of data used in intra-variation calculations for *Ammothea glacialis*, *Colossendeis megalonyx*, and *Nymphon australe*: pore length (µm), pore diameter (µm), and conductance (µmol s^{-1} kPa^{-1} $pore^{-1}$)

species	individual	leg segment	pore length	pore diameter	total # pores	Conductance*	
						water model	tissue model
Ammothea glacialis	ind1	femur	85.83	11.75	19778	1.09E-10	8.02E-11
		1 tibia	69.05	13.20	25510	3.30E-11	3.00E-11
		2 tibia	79.40	14.47	28420	4.69E-11	4.08E-11
Ammothea glacialis	ind2	femur	68.19	12.62	22817	5.73E-11	4.86E-11
		1 tibia	68.64	14.31	24032	4.27E-11	3.86E-11
		2 tibia	69.95	11.44	22551	2.88E-11	2.48E-11
Ammothea glacialis	ind3	femur	72.65	13.45	18741	7.54E-11	6.00E-11
		1 tibia	68.90	15.24	20736	3.54E-11	3.17E-11
		2 tibia	70.24	15.45	21324	2.64E-11	2.43E-11
Ammothea glacialis	ind4	femur	68.29	12.86	25130	3.81E-11	3.33E-11
		1 tibia	63.71	14.27	20795	6.04E-11	5.04E-11
		2 tibia	65.52	12.68	25245	4.31E-11	3.86E-11
Ammothea glacialis	ind5	femur	70.34	11.09	19412	5.39E-11	4.45E-11
		1 tibia	64.13	10.72	18619	6.80E-11	5.60E-11
		2 tibia	55.53	14.01	24368	2.89E-11	2.56E-11
Ammothea glacialis	ind6	femur	73.60	14.16	25357	7.83E-11	6.49E-11
		1 tibia	72.01	17.11	22792	3.22E-11	2.96E-11
		2 tibia	88.43	14.84	24903	5.10E-11	4.21E-11
Ammothea glacialis	ind7	femur	75.48	14.38	24235	4.58E-11	3.84E-11

		1 tibia	53.01	14.47	26309	3.72E-11	3.28E-11
		2 tibia	78.77	12.75	23390	2.82E-11	2.48E-11
Ammothea glacialis	ind8	femur	69.32	12.98	21027	3.31E-11	2.96E-11
		1 tibia	78.16	13.81	21633	6.21E-11	5.23E-11
		2 tibia	41.90	15.69	23993	4.70E-11	4.13E-11
Colossendeis megalonyx	ind1	femur	55.34	20.25	20893	4.68E-11	4.20E-11
		1 tibia	51.87	25.59	22300	1.32E-10	1.16E-10
		2 tibia	59.21	23.93	23057	6.72E-11	6.22E-11
Colossendeis megalonyx	ind2	femur	55.01	29.23	27162	6.31E-11	5.87E-11
		1 tibia	49.60	26.32	25879	6.63E-11	6.24E-11
		2 tibia	53.13	23.92	25573	4.59E-11	4.26E-11
Colossendeis megalonyx	ind3	femur	50.22	27.81	20289	1.09E-10	9.97E-11
		1 tibia	49.47	19.09	22287	4.98E-11	4.65E-11
		2 tibia	54.95	28.23	22166	4.81E-11	4.53E-11
Colossendeis megalonyx	ind4	femur	61.29	26.93	22466	9.34E-11	8.50E-11
		1 tibia	59.82	26.42	23379	3.93E-11	2.95E-11
		2 tibia	55.48	26.39	27076	5.77E-11	5.42E-11
Colossendeis megalonyx	ind5	femur	45.29	30.09	32158	1.01E-10	9.31E-11
		1 tibia	52.87	33.57	29447	1.59E-10	1.42E-10
		2 tibia	47.26	28.21	31030	4.93E-11	4.67E-11
Colossendeis megalonyx	ind6	femur	46.63	22.00	31638	1.16E-10	1.03E-10
		1 tibia	43.12	21.51	29432	2.48E-11	2.36E-11
		2 tibia	52.62	26.26	32783	4.50E-11	4.24E-11
Colossendeis megalonyx	ind7	femur	60.47	24.82	23968	1.01E-10	8.85E-11
		1 tibia	54.99	22.46	29425	2.30E-11	2.18E-11
		2 tibia	59.96	24.95	31096	2.89E-11	2.75E-11
Colossendeis megalonyx	ind8	femur	50.69	24.12	32500	4.62E-11	4.29E-11
		1 tibia	48.78	17.35	27507	7.26E-11	6.56E-11
		2 tibia	54.94	18.60	27290	5.90E-11	5.33E-11
Nymphon australe	ind1	femur	16.44	5.49	26780	1.71E-10	1.06E-10
		1 tibia	10.00	7.27	18196	2.35E-10	1.72E-10
		2 tibia	25.00	6.12	23748	1.60E-10	9.97E-11
Nymphon australe	ind2	femur	9.49	5.37	10623	3.19E-10	1.99E-10
		1 tibia	10.00	5.82	10503	1.04E-10	8.28E-11
		2 tibia	10.00	4.73	22427	1.15E-10	8.84E-11
Nymphon australe	ind3	femur	20.00	8.81	23216	2.96E-10	2.08E-10

		1 tibia	40.00	7.06	16932	1.84E-10	1.13E-10
		2 tibia	30.00	6.13	22188	1.51E-10	9.75E-11
Nymphon australe	ind4	femur	NA	NA	17692	NA	NA
		1 tibia	NA	NA	9194	NA	NA
		2 tibia	20.00	5.68	18223	1.13E-10	8.30E-11
Nymphon australe	ind5	femur	NA	NA	11261	NA	NA
		1 tibia	NA	NA	23664	NA	NA
		2 tibia	NA	NA	19630	NA	NA
Nymphon australe	ind6	femur	NA	NA	19057	NA	NA
		1 tibia	NA	NA	15866	NA	NA
		2 tibia	NA	NA	16609	NA	NA
Nymphon australe	ind7	femur	NA	NA	9793	NA	NA
		1 tibia	NA	NA	19133	NA	NA
		2 tibia	NA	NA	15884	NA	NA
Nymphon australe	ind8	femur	NA	NA	17525	NA	NA
		1 tibia	NA	NA	22765	NA	NA
		2 tibia	NA	NA	21978	NA	NA

*Conductance was calculated based on the 2 different models used to calculate resistance. One with the diffusion coefficient of water and one with the diffusion coefficient of tissue. See text for more details

Table S4. Summary of data used in scaling analyses and calculating flux: pore length (x, µm), pore diameter (d, µm), resistance (R, kPa s µmol^{-1}), and pore density (P, pores cm^{-2})

			water model	tissue model	
Species	x	d	R	R	P
Ammotheidae					
Ammothea glacialis	85.83	12.98	9.17E+09	1.25E+10	19778
	68.19	14.38	1.75E+10	2.06E+10	22817
	72.65	11.54	1.33E+10	1.67E+10	18741
	68.29	10.32	2.62E+10	3.00E+10	25130
	70.34	11.63	1.85E+10	2.24E+10	19412
	73.60	13.45	1.28E+10	1.54E+10	25357
	75.48	9.44	2.18E+10	2.60E+10	24235
	69.32	10.74	3.02E+10	3.38E+10	21027
Ammothea longispina	73.14	9.79	9.02E+09	1.33E+10	32038
	71.36	12.60	3.10E+10	3.46E+10	23689
Ammothea sp	33.31	6.83	4.84E+09	7.21E+09	12662
	43.36	9.34	7.78E+09	1.32E+10	NA
Colossendeidae					
Colossendeis hoeki	89.13	21.98	2.05E+10	2.20E+10	28047
	108.38	23.38	4.92E+10	5.20E+10	NA
Colossendeis megalonyx	55.34	24.12	2.14E+10	2.38E+10	20893

	55.01	24.82	1.58E+10	1.70E+10	27162
	50.22	22.00	9.15E+09	1.00E+10	20289
	61.29	30.09	1.07E+10	1.18E+10	22466
	45.29	26.93	9.89E+09	1.07E+10	32158
	46.63	27.81	8.60E+09	9.70E+09	31638
	60.47	29.23	9.86E+09	1.13E+10	23968
	50.69	20.25	2.17E+10	2.33E+10	32500
Colossendeis scotti	99.68	43.62	8.61E+09	9.13E+09	14842
	130.33	51.27	7.03E+09	8.03E+09	15854
Nymphonidae					
Nymphon australe	16.44	5.49	5.83E+09	9.47E+09	26780
	9.49	5.37	3.14E+09	5.03E+09	10623
	20.00	8.81	3.37E+09	4.82E+09	23216
	NA	NA	NA	NA	17692
	NA	NA	NA	NA	11261
	NA	NA	NA	NA	19057
	NA	NA	NA	NA	9793
	NA	NA	NA	NA	17525
Pentanymphon antarcticum	9.81	2.48	4.49E+10	5.88E+10	28811
	21.46	3.30	9.84E+10	1.19E+11	NA
Pallenopsidae					
Pallenopsis patagonica	10.95	4.32	1.29E+10	1.61E+10	25529
	13.76	5.77	4.38E+09	6.51E+09	NA
Pycnogonidae					
Pycnogonum gaini	122.71	31.24	4.21E+09	4.99E+09	2355
	135.44	32.35	9.23E+09	1.05E+10	NA

Table S5. Summary of mass (M, g), surface area (A, cm^2), and oxygen gradient (ΔPO_2) data for individuals used in scaling analyses and calculating flux and total pore number.

Species	*M*	*A*	*ΔPO₂*
Ammotheidae			
Ammothea glacialis	1.60	28.480	5.16
	1.07	20.457	8.9
	1.32	25.352	6.86
	1.36	27.594	4.15
Ammothea longispina	0.510	14.837	7.55
	0.647	16.893	6.16
	0.664	16.783	6.68
Ammothea sp.	3.54	47.219	3.16
	3.11	45.310	3.61
Colossendeidae			
Colossendeis hoeki	1.22	29.076	2.04
	0.982	23.299	7.47
	1.13	20.740	7.94
Colossendeis megalonyx	2.20	49.675	8.88

	2.54	62.831	6.61
	0.470	17.458	3.29
	1.10	31.745	NA
Colossendeis scotti	12.60	118.692	5.5
	8.39	109.837	10.4
	8.40	96.304	9
Nymphonidae			
Nymphon australe	0.140	7.819	NA
	0.160	4.898	0.82
	0.100	5.338	1.43
	0.070	3.674	0.27
	0.190	6.245	2.73
	0.090	5.307	NA
	0.070	4.553	NA
Pentanymphon antarcticum	0.035	3.799	2.13
	0.068	5.495	3.94
	0.069	6.390	5.13
	0.036	3.941	1.26
Pallenopsidae			
Pallenopsis patagonica	0.776	19.295	4.51
	0.395	10.582	5.17
	0.469	12.733	3.18
Pycnogonidae			
Pycnogonum gaini	0.618	10.833	NA
	0.440	8.368	6.26
	0.543	8.161	5.11

Table S6. Summary of average component resistances (kpa s µmol^{-1}) for each layer of model for each species.

Species	Rtop	Rcut	water model Rseg	tissue model Rseg	water model Rbot	tissue model Rbot	water model Rtot	tissue model Rtot
Ammothea glacialis	2.04E+08	1.61E+10	2.29E+09	5.72E+09	4.88E+07	1.22E+08	1.87E+10	2.22E+10
Ammothea longispina	2.27E+08	1.71E+10	2.58E+09	6.45E+09	5.06E+07	1.26E+08	2.00E+10	2.39E+10
Ammothea sp	1.40E+08	3.55E+09	2.54E+09	6.35E+09	7.52E+07	1.88E+08	6.31E+09	1.02E+10
Colossendeis hoeki	2.33E+08	3.32E+10	1.40E+09	3.50E+09	3.71E+07	9.27E+07	3.48E+10	3.70E+10
Colossendeis megalonyx	2.22E+08	1.23E+10	8.60E+08	2.15E+09	2.90E+07	7.24E+07	1.34E+10	1.47E+10
Colossendeis scotti	9.82E+07	7.22E+09	4.88E+08	1.22E+09	1.36E+07	3.40E+07	7.82E+09	8.58E+09
Nymphon australe	1.81E+08	2.38E+09	1.40E+09	3.50E+09	1.52E+08	3.79E+08	4.11E+09	6.44E+09
Pentanymphon antarcticum	8.36E+08	5.94E+10	1.12E+10	2.80E+10	2.08E+08	5.19E+08	7.16E+10	8.87E+10
Pallenopsis patagonica	2.70E+08	6.61E+09	1.59E+09	3.98E+09	1.75E+08	4.37E+08	8.65E+09	1.13E+10
Pycnogonum gaini	1.01E+08	5.94E+09	6.59E+08	1.64E+09	2.30E+07	5.73E+07	6.72E+09	7.74E+09